Rodríguez-Martínez, J.A.; Vadillo, G.; Zaera, R.; Fernández-Sáez, J.; Rittel, D. (2015). An analysis of microstructural and thermal softening effects in dynamic necking. *Mechanics of Materials*, vol. 80, part B, pp. 298-310.

DOI: https://doi.org/10.1016/j.mechmat.2013.10.011

An analysis of microstructural and thermal softening effects in dynamic necking inception

J. A. Rodríguez-Martínez[a], G. Vadillo[a,*], R. Zaera[a], J. Fernández-Sáez[a], D. Rittel[b,a]

[a] *Department of Continuum Mechanics and Structural Analysis. University Carlos III of Madrid. Avda. de la Universidad, 30. 28911 Leganés, Madrid, Spain*
[b] *Faculty of Mechanical Engineering, Technion, 32000, Haifa, Israel*

Abstract

The competition between material and thermal induced destabilizing effects in dynamic shear loading has been previously addressed in detail using a fully numerical approach in Osovski et al. (2013). This paper presents an analytical solution to the related problem of dynamic tensile instability in a material that undergoes both twinning and dynamic recrystallization. A special prescription of the initial and loading conditions precludes wave propagation in the specimen which retains nevertheless its inertia. This allows for a clear separation of material vs. structural effects on the investigated localization. The outcome of this analysis confirms the dominant role of microstructural softening in the lower strain-rate regime (of the order of 10^3 s^{-1}), irrespective of the extent of prescribed thermal softening. By contrast, the high strain-rate regime is found to be dominated by inertia as a stabilizing factor, irrespective of the material's thermo-physical conditions, a result that goes along the predictions of Rodríguez-Martínez et al. (2013a) regarding dynamically expanding rings.

Keywords: dynamic necking, linear stability analysis, numerical simulation, dynamic recrystallization, thermal softening

1. Introduction

Recrystallization is a process in which nucleation and growth of new strain-free grains, assumed to occur on grain boundaries, replace the deformed microstructure of a strained

*Corresponding author. Tel. +34916248460; Fax: +34 916249430. E-mail address: gvadillo@ing.uc3m.es

material. Together with slip, recovery, grain growth or phase transformation, it is one of the most important microstructural evolution processes. Recrystallization may occur after deformation, the post-deformation annealing process called *static* recrystallization, or during deformation. The latter is termed *dynamic* recrystallization (DRX), and it takes place in many alloys when they deform at high strains and high strain rates (Tanner and McDowell, 1999; Qu et al., 2005; Medyanik et al., 2007; Osovski and Rittel, 2012; Li et al., 2013). DRX initiates upon reaching a critical condition. The two most widely accepted criteria for the onset of DRX make use of a critical strain (Fan and Yang, 2011) or a critical dislocation density (Bailey and Hirsch, 1962; Ding and Guo, 2001). The last criterion is equivalent to a critical stored energy if the stored energy is assumed to be a function of dislocation density only (Brown and Bammann, 2012). Thus, Rittel et al. (2006, 2008) suggested to consider the dynamically stored energy of cold work, namely the part of the energy that is not dissipated into heat, as a criterion for the onset of dynamic recrystallization (DRX), which may appear long before final failure. Recently, Medyanik et al. (2007) proposed a criterion for the onset of DRX deformation mechanism, formulated in terms of temperature. This approach, however, still requires elevated temperatures as a trigger for DRX (0.4 to 0.5 of melting temperature), while this requirement stands in contradiction with some of the experimental observations reported by Rittel and Wang (2008).

When the critical value for the onset of DRX is reached, the elimination of dislocations reduces the stored energy, resulting in a decrease of flow stress, hardness and a simultaneous increase in the ductility (Ganapathysubramanian and Zabaras, 2004; Fan and Yang, 2011; Brown and Bammann, 2012). As a result, the material locally softens giving rise to inhomogeneous deformation patterns which can, in turn, be important precursors to plastic instabilities. Regarding dynamic shear loading conditions, Rittel et al. (2006, 2008) suggested that the onset of the so-called "adiabatic shear bands" is primarily related to microstructural transformations which were indeed observed long before any significant self-heating of the material develops. The formation of dynamically recrystallized grains, which may appear long before final failure, creates soft enclaves in the surrounding hardening material. Final failure occurs therefore as a result of the growth and coalescence of

islands of dynamically recrystallized phase, as shown by Osovski et al. (2012b). Moreover, if DRX is present it may override thermal softening effects, thus emerging as the main cause of ASBs (Osovski et al., 2013) in materials that exhibit early DRX (e.g. Ti6Al4V alloy).

In parallel to adiabatic shear banding, which was considered by the above authors to analyze the respective influence of microstructural and thermal softening, dynamic necking represents a paradigmatic case of plastic instability occurring at high strain rates. Dynamic necking is known to be strongly affected by thermal effects since the deformation process approaches adiabaticity. In such conditions, the thermal softening of the material appears to be a critical factor for localization (Klepaczko, 1968; Fressengeas and Molinari, 1985). In materials with a strong thermal softening, the temperature increase may dictate the conditions for stability, on top of other softening effects. However, following the results by Rittel and co-workers for a shear stress state (Rittel et al., 2008; Osovski and Rittel, 2012; Osovski et al., 2012a,b, 2013), it is worth analyzing the respective influence of microstructural and thermal softening in dynamic necking inception.

In this work, the role of both microstructural and thermal softening on the localization of plastic deformation in dynamically stretching rods is examined. Two different modeling methodologies are used: Linear stability technique derived within a quasi-1D theoretical framework and finite element simulations of slender bars subjected to uniaxial tension. The constitutive equation accounts for hardening due to twinning and softening – dynamic recrystallization– microstructural effects, as well as for thermal softening of the material. A parametric study, performed on the constants of the constitutive model, driving these effects, allows for the identification of their relative role in the onset of dynamic necking.

2. Constitutive model

The constitutive model uses Huber-Mises plasticity as in the previous work of Osovski et al. (2013). The model considers three possible mechanisms responsible for the plastic flow: Slip, twinning and dynamic recrystallization. Those three mechanisms are treated using a rule of mixture to describe the mechanical, microstructural and thermal evolution of the material. In the undeformed configuration the material is only formed by the slip

phase. Twinning is triggered by plastic deformation and complements dislocation activity increasing the material flow stress and strain hardening. Twinning is assumed to stop once DRX starts, whose onset is determined by a threshold value of the stored energy of cold work. Dynamic recrystallization contributes to the material strain softening. It should be noted that the material is considered strain rate independent in order to facilitate interpretation of the respective influence that microstrutural and thermal softening effects have on flow localization.

In this paper, flow localization in a rapidly stretched bar is analyzed using linear stability -derived within a 1D framework– and finite element simulations –developed within a 3D framework-. Therefore one-dimensional and three-dimensional approaches will be presented, understanding that both coincide in their essential features and that, for a uniaxial state of stress, the 3D model provides the same results as its 1D counterpart.

2.1. 1D model

The material constitutive equations of the problem were presented in Osovski et al. (2013) and will only be repeated here for the sake of clarity. The effective yield stress is calculated by the following expression:

$$\sigma_y = \Psi\left(\bar{\varepsilon}^p, T\right) = h\left(\bar{\varepsilon}^p\right) p\left(T\right) \tag{1}$$

where the functions $h\left(\bar{\varepsilon}^p\right)$ and $p\left(T\right)$ gather the strain $\bar{\varepsilon}^p$ and temperature T dependencies of the material, which are defined as follows:

- The function $h\left(\bar{\varepsilon}^p\right)$ is composed by three terms and reads as follows:

$$h\left(\bar{\varepsilon}^p\right) = \left(1 - f_{DRX}\right)\sigma_y^0 + f_{DRX}\sigma_y^{DRX} + \left(1 - f_{DRX} - f_{twins}\right) \left(K_t\left(\frac{1}{\chi}\right) + K_d\left(\bar{\varepsilon}^p\right)^n\right) \tag{2}$$

  where f_{DRX} and f_{twins} are the volume fractions of DRX and twins respectively. The first yield stress term in the previous expression represents the initial yield stress of

the material –which is controlled by the slip phase– and it is defined by σ_y^0. The second yield stress term is to be understood as the flow stress at which DRX first appears (upon reaching the energetic threshold given by U_{DRX}, see Eqs. (3)-(4)) which is determined by the parameter $\sigma_y^{DRX} = \sigma_y|_{U=U_{DRX}}$ (to be calculated in the integration procedure for each loading case). The third yield stress term is an isotropic strain hardening function which consists of two parts: (a) the contribution of evolving density of twins, acting as barriers for dislocation motion, enters the equation as a Hall-Petch like term, where K_t is a strain hardening parameter and χ is the average distance between twins given by $\chi = \frac{2t(1-f_{twins})}{f_{twins}}$ with t being the average twin width; and (b) the strain hardening resulting from dislocation activity during deformation with K_d being the strain hardening parameter and n the strain hardening exponent.

The evolution law for the twins volume fraction is as follows:

$$f_{twins} = g\left(\bar{\varepsilon}^p\right) = \begin{cases} \frac{1}{N}\left[\arctan\left(2\pi a\bar{\varepsilon}^p - 2\pi b\right) - \arctan\left(-2\pi b\right)\right]; & U < U_{DRX} \\ f^*_{twins} = f_{twins}|_{U=U_{DRX}}; & U \geqslant U_{DRX} \end{cases} \tag{3}$$

where U is the stored energy of cold work (see Eq. (5)) and U_{DRX} is the threshold energy for the onset of the recrystallization process. Here, a, b and N are material parameters to reproduce the average number of twins per grain measured at different strains.

The evolution law for the DRX volume fraction is defined by:

$$f_{DRX} = w\left(U\right) = \begin{cases} 0; & U < U_{DRX} \\ 1 - \exp\left(-k_{DRX}\left(\frac{U-U_{DRX}}{U_{DRX}}\right)^{n_{DRX}}\right); & U \geqslant U_{DRX} \end{cases} \tag{4}$$

where k_{DRX} and n_{DRX} are material parameters which describe the volume fraction of DRX upon plastic strain.

The stored energy is calculated by:

$$U = (1 - f_{DRX} - f_{twins})(1 - \beta) \int_0^{\bar{\varepsilon}^p} \bar{\sigma} d\bar{\varepsilon}^p \tag{5}$$

where β is the Taylor-Quinney coefficient of the phase undergoing slip which is assumed as constant and $\bar{\sigma}$ is the equivalent stress.

- The function $p(T)$ reads as follows:

$$p(T) = (1 - \alpha \Delta T) \tag{6}$$

where α is the temperature sensitivity parameter and $\Delta T = T - T_0$, being T the current temperature and T_0 the initial temperature. The linear dependence shown in the above equation is the simplest dependence one can think of, yet being physical to some extent.

The yield condition may be written as

$$\Phi = \bar{\sigma} - \Psi(\bar{\varepsilon}^p, T) = 0 \tag{7}$$

2.2. 3D model

The previous 1D constitutive model can be extended to a 3D framework. Here, the above equations are complemented with the generalized Hooke's law for hypoelastic-plastic materials:

$$\boldsymbol{\sigma}^{\nabla} = \mathbf{C} : \mathbf{d}^e = \mathbf{C} : (\mathbf{d} - \mathbf{d}^p) \tag{8}$$

where $\boldsymbol{\sigma}^{\nabla}$ is an objective derivative of the Cauchy stress tensor, $\mathbf{d}$, $\mathbf{d}^e$ and $\mathbf{d}^p$ are respectively the total, elastic, and inelastic rate of deformation tensors, and $\mathbf{C}$ is the isotropic elastic tensor, defined by the elastic constants K and G. Additionally, an associated flow rule is considered

$$\mathbf{d}^p = \dot{\lambda}\frac{\partial \Phi}{\partial \boldsymbol{\sigma}} = \dot{\lambda}\frac{3}{2}\frac{\mathbf{s}}{\bar{\sigma}} \tag{9}$$

λ being the plastic multiplier, which coincides with the equivalent plastic strain in Huber-Mises plasticity, and $\mathbf{s}$ being the deviatoric stress tensor.

The plastic part of the macroscopic strain rate and the effective plastic strain rate are related by enforcing the equality between macroscopic and effective plastic work rates as:

$$\sigma^{\nabla} : \mathbf{d}^p = \bar{\sigma}\dot{\bar{\varepsilon}}^p \tag{10}$$

The formulation of the model is completed by introducing the Kuhn-Tucker loading/unloading complementary conditions:

$$\dot{\lambda} \geq 0, \quad \Phi \leq 0, \quad \dot{\lambda}\Phi = 0 \tag{11}$$

and the consistency condition during plastic loading:

$$\dot{\Phi} = 0 \tag{12}$$

Table 1 shows the values of the model parameters, as taken from Osovski et al. (2013).

3. Problem formulation and linear stability analysis

3.1. Governing equations

The problem addressed is based on the configuration reported in Zhou et al. (2006). A cylindrical bar of length L_0, cross section radius r_0 and area $A_0 = \pi r_0^2$ is considered. The bar is subjected to a constant stretching velocity on both sides. It is supposed that this loading condition is always satisfied, and therefore elastic unloading is disregarded. The bar material is taken to be incompressible, of mass density ρ_0, with a constitutive behaviour described by Eqs.(1-7).

The true strain ε and the strain rate $\dot{\varepsilon}$ are defined as $\varepsilon = ln\left[(\partial x/\partial X)_t\right]$ and $\dot{\varepsilon} = \partial\varepsilon/\partial t$, X being the Lagrangian coordinate ($-L_0/2 \leq X \leq L_0/2$), and x the Eulerian coordinate given by

Symbol	Property and units	Value
σ_y^0	Initial yield stress (MPa), Eq.(3)	500
K_t	Strain hardening parameter ($mMPa$), Eq.(3)	1.8×10^{-3}
t	Average twin width (μm), Eq.(3)	2
K_d	Strain hardening parameter (MPa), Eq.(3)	215
n	Strain hardening exponent, Eq.(3)	0.25
α^*	Reference temperature sensitivity parameter (K^{-1}), Eq.(6)	10^{-4}
T_0	Initial temperature (K), Eq.(6)	293
N	Material parameter, Eq.(3)	7.4594
a	Material parameter, Eq.(3)	5
b	Material parameter, Eq.(3)	1
U^*	Reference threshold energy for DRX formation (MPa/m^3), Eqs.(3-4)	92
k_{DRX}	Material parameter, Eq.(4)	0.5
n_{DRX}	Material parameter, Eq.(4)	8.7
G	Elastic shear modulus (GPa)	43.6
K	Elastic bulk modulus (GPa)	116
β	Taylor-Quinney coefficient, Eqs.(5,20)	0.6
k	Thermal conductivity (W/mK), Eq.(20)	21.9
l_h	Transformation latent heat (MJ/m^3), Eq.(20)	118
ρ_0	Density (kg/m^3), Eq.(20)	4500
c	Specific heat (MJ/m^3K), Eq.(20)	234

Table 1: *Parameters related to yield stress, DRX and twins volume fractions, stiffness parameters, and conventional material constants representative of titanium alloys as taken from Osovski et al. (2013).*

$$x = X + \int_0^t v(X,\tau)d\tau \tag{13}$$

where v is the current axial velocity. Since large deformations are considered, elasticity can be neglected. Note that for considering uniaxial tensile conditions, $\bar{\varepsilon}^p = \varepsilon$.

The fundamental equations governing the loading process are presented below:

- Mass conservation:

$$\frac{\partial v}{\partial X} = e^{\varepsilon}\dot{\varepsilon} \tag{14}$$

- Momentum balance in the axial direction:

$$\rho\frac{\partial v}{\partial t} = \frac{\partial}{\partial X}(\sigma e^{-\varepsilon}) \tag{15}$$

- Flow stress:

$$\sigma = \left(1+\theta^{-1}\right) ln(1+\theta)\sigma_y \tag{16}$$

where σ is the true stress, defined as the averaged axial stress in the cross-section. The correction factor θ (Bridgman, 1952; Walsh, 1984; Fressengeas and Molinari, 1985) is used to take into account that, in case of necking, the local axial stress is enhanced by the hydrostatic stress. The factor θ is defined as

$$\theta = \frac{1}{2}r\left(\frac{\partial^2 r}{\partial x^2}\right) = \frac{2A\left(\frac{\partial^2 A}{\partial x^2}\right) - \left(\frac{\partial A}{\partial x}\right)^2}{8\pi A} = \frac{A_0 e^{-3\varepsilon}}{8\pi}\left(\left(\frac{\partial \varepsilon}{\partial X}\right)^2 - \frac{\partial^2 \varepsilon}{\partial X^2}\right) \tag{17}$$

where the relation $A = A_0 e^{-\varepsilon}$, derived from the incompressibility condition, has been used.

- Twinning transformation law: from Eq. (3)

$$f_{twins} = g\left(\varepsilon\right) \tag{18}$$

- DRX transformation law: from Eq. (4)

$$f_{DRX} = w\left(U\right) \tag{19}$$

- Conservation of energy: assuming no heat flow at the specimen's boundaries (a slender bar subjected to rapid stretching will be analysed as further described in section 4) and neglecting the contribution of thermoelastic effects :

$$c\frac{\partial T}{\partial t} = \beta\sigma\dot{\varepsilon} + k\frac{\partial^2 T}{\partial x^2} + \frac{\partial f_{DRX}}{\partial t}l_h \tag{20}$$

where c, k and l_h stand for the heat capacity per unit volume, the thermal conductivity and the latent heat per unit volume of transformed DRX due to the exothermic character of the phase transformation (Zaera et al., 2013a). Note that in uniaxial stress conditions $\bar{\sigma} = \sigma$.

Considering the domain $[-L_0/2, L_0/2]$, the equations (14-16) and (18-20) are to be solved under the following initial conditions formulated in Lagrangian coordinates:

$$\begin{aligned} &v(X,0) = \dot{\varepsilon}_0 X \\ &\sigma(X,0) = \Psi\left(0\right) = \sigma_y^0 \\ &\varepsilon(X,0) = 0 \\ &T(X,0) = T_0 \\ &f_{twins}(X,0) = 0 \\ &f_{DRX}(X,0) = 0 \end{aligned} \tag{21}$$

and boundary conditions:

$$\begin{aligned} &v(L_0/2,t) = -v(-L_0/2,t) = \dot{\varepsilon}_0 L_0/2 \\ &\partial T(X,t)/\partial X|_{X=L_0/2} = \partial T(X,t)/\partial X|_{X=-L_0/2} = 0 \end{aligned} \tag{22}$$

The constant $\dot{\varepsilon}_0$ defines the value of the initial strain rate in the bar.

3.2. Linear perturbation analysis

Let $\mathbb{S}(X,t) = (v(X), \sigma(t), \varepsilon(t), T(t), f_{twins}(t), f_{DRX}(t))^T$ be the fundamental time-dependent solution, at time t, of the previous problem. $\mathbb{S}$ is obtained by integration of Eqs. (14-16) and (18-20) satisfying the initial and boundary conditions previously listed.

At time $t = t_1$, at which the fundamental solution reaches the value $\mathbb{S}_1(X,t_1) = (v_1(X), \sigma_1, \varepsilon_1, T_1, f_{twins1}, f_{DRX1})^T$, consider a small perturbation of this solution $\delta\mathbb{S}(X,t)_{t_1}$, with $|\delta\mathbb{S}(X,t)_{t_1}| \ll |\mathbb{S}_1(X,t_1)|$, given by

$$\delta\mathbb{S}(X,t)_{t_1} = \delta\mathbb{S}_1 e^{i\xi X} e^{\eta(t-t_1)} \tag{23}$$

where $\delta\mathbb{S}_1 = (\delta v, \delta\sigma, \delta\varepsilon, \delta T, \delta f_{twins}, \delta f_{DRX})^T$ is the perturbation amplitude, ξ the wavenumber and η the growth rate of the perturbation at time t_1. The perturbation becomes unstable when $Re(\eta) > 0$. According to Rodríguez-Martínez et al. (2013b) the perturbation growth η^+ is assumed to represent the onset of *diffuse necking*, the very first stages at which the local plastic flow deviates from the background value.

By substituting Eq. (23) into Eqs. (14-16) and (18-20) and retaining only first-order terms, the following linearized equations are obtained:

- Mass conservation:

$$\delta v + i\xi^{-1} e^{\varepsilon_1} \left(\dot{\varepsilon}_1 + \eta\right) \delta\varepsilon = 0 \tag{24}$$

- Momentum balance in the axial direction:

$$\rho\eta\delta v - i\xi e^{-\varepsilon_1}\delta\sigma + i\xi\sigma_1 e^{-\varepsilon_1}\delta\varepsilon = 0 \tag{25}$$

Concerning the value of the stored energy of cold work, there are two possible scenarios, for the remaining equations, depending on the perturbation time:

1. The perturbation time t_1 is such that $U < U_{DRX}$

- Flow stress:

$$\delta\sigma - (\sigma_1 \frac{A_0\xi^2}{8\pi} e^{-3\varepsilon_1} + H)\delta\varepsilon - P\delta T - R\delta f_{twins} = 0 \tag{26}$$

- Twinning transformation law:

$$\delta f_{twins} - G\delta\varepsilon = 0 \tag{27}$$

- DRX transformation law:

$$\delta f_{DRX} = 0 \tag{28}$$

- Conservation of energy:

$$\beta\dot{\varepsilon}_1\delta\sigma + \beta\sigma_1\eta\delta\varepsilon - (c\eta + k\xi^2)\delta T = 0 \tag{29}$$

2. The perturbation time t_1 is such that $U \geqslant U_{DRX}$

- Flow stress:

$$\delta\sigma - (\sigma_1 \frac{A_0\xi^2}{8\pi} e^{-3\varepsilon_1} + H)\delta\varepsilon - P\delta T - Q\delta f_{DRX} = 0 \tag{30}$$

- Twinning transformation law:

$$\delta f_{twins} = 0 \tag{31}$$

- DRX transformation law:

$$\delta f_{DRX} - W\delta U = 0 \tag{32}$$

where δU is obtained linearising Eq. (5) as follows:

$$\delta U = -(1-\beta)E_p\,\delta f_{DRX} + (1 - f_{DRX1} - f_{twins1})\,(1-\beta)\sigma_1\delta\varepsilon \tag{33}$$

- Conservation of energy:

$$\beta\dot{\varepsilon}_1\delta\sigma + \beta\sigma_1\eta\delta\varepsilon - (c\eta + k\xi^2)\delta T + l_h\eta\delta f_{DRX} = 0 \tag{34}$$

in Eqs. (24-34) the following definitions have been used

$$H = \left.\frac{\partial\Psi}{\partial\varepsilon}\right|_{t_1}\;; \quad P = \left.\frac{\partial\Psi}{\partial T}\right|_{t_1}\;; \quad Q = \left.\frac{\partial\Psi}{\partial w}\right|_{t_1}\;; \quad R = \left.\frac{\partial\Psi}{\partial g}\right|_{t_1}$$

$$G = \left.\frac{\partial g}{\partial\varepsilon}\right|_{t_1}\;; \quad W = \left.\frac{\partial w}{\partial U}\right|_{t_1}\;; \quad E_p = \int_0^{\varepsilon_1}\sigma d\varepsilon$$

A non-trivial solution for $\delta\mathbb{S}_1$ is obtained only if the determinant of the systems of linear algebraic equations (24-29) or (24-25) and (30-34) is equal to zero. Using the following dimensionless variables and constants

$$\bar{\eta} = \frac{\eta}{\dot{\varepsilon}_1}\;; \quad \bar{\xi} = r_0\xi\;; \quad \psi(\varepsilon, T) = \frac{\Psi(\varepsilon, T)}{\sigma_y^0}$$

$$\bar{I} = \sqrt{\frac{\sigma_y^0}{\rho r_0^2\dot{\varepsilon}_1^2}}\;; \quad \Lambda = e^{-\varepsilon_1}\;; \quad \psi_1 = \frac{\sigma_1(t_1)}{\sigma_y^0}\;; \quad \bar{l}_h = l_h\frac{1}{\sigma_y^0}$$

$$\tilde{H} = H\frac{1}{\sigma_y^0}\;; \quad \tilde{P} = P\frac{T_0}{\sigma_y^0}$$

$$\tilde{Q} = Q\frac{1}{\sigma_y^0}\;; \quad \tilde{R} = R\frac{1}{\sigma_y^0}\;; \quad \tilde{G} = G\;; \quad \tilde{W} = W\frac{(1 - f_{DRX1} - f_{twins1})\,(1-\beta)\,\sigma_1}{W\,(1-\beta)\,E_p\; + 1}$$

$$\tilde{c} = c\frac{T_0}{\sigma_y^0} \; ; \quad \tilde{k} = k\frac{T_0}{\sigma_y^0 \dot{\varepsilon}_1 r_0^2}$$

The resulting condition is found to be a cubic equation in $\bar{\eta}$

$$B_3\bar{\eta}^3 + B_2\bar{\eta}^2 + B_1\bar{\eta} + B_0 = 0 \tag{35}$$

with

$$B_3 = \tilde{c} \tag{36}$$

$$B_2 = \bar{\xi}^2\tilde{k} + \tilde{c} - \tilde{P}\beta \tag{37}$$

with B_1 and B_0 depending on the perturbation time, namely:

1. The perturbation time t_1 is such that $U < U_{DRX}$

$$B_1 = \Lambda^2\bar{\xi}^2\bar{I}^2(\tilde{c}\tilde{H} + \tilde{c}\tilde{G}\tilde{R} - \tilde{c}\psi_1 + \beta\tilde{P}\psi_1 + \tfrac{\tilde{c}}{8}\Lambda^3\psi_1\bar{\xi}^2) - \beta\tilde{P} + \tilde{k}\bar{\xi}^2 \tag{38}$$

$$B_0 = \Lambda^2\bar{\xi}^2\bar{I}^2(\beta\tilde{P}\psi_1 + \tilde{H}\tilde{k}\bar{\xi}^2 + \tilde{G}\tilde{k}\tilde{R}\bar{\xi}^2 - \tilde{k}\psi_1\bar{\xi}^2 + \frac{\tilde{k}}{8}\Lambda^3\psi_1\bar{\xi}^4) \tag{39}$$

2. The perturbation time t_1 is such that $U \geqslant U_{DRX}$

$$B_1 = \Lambda^2\bar{\xi}^2\bar{I}^2(\tilde{c}\tilde{H} + \tilde{c}\tilde{W}\tilde{Q} - \tilde{c}\psi_1 + \beta\tilde{P}\psi_1 + \tfrac{\tilde{c}}{8}\Lambda^3\psi_1\bar{\xi}^2 + \tilde{W}\bar{l}_h\tilde{P}) - \beta\tilde{P} + \tilde{k}\bar{\xi}^2 \tag{40}$$

$$B_0 = \Lambda^2\bar{\xi}^2\bar{I}^2(\beta\tilde{P}\psi_1 + \tilde{H}\tilde{k}\bar{\xi}^2 + \tilde{W}\tilde{k}\tilde{Q}\bar{\xi}^2 - \tilde{k}\psi_1\bar{\xi}^2 + \frac{\tilde{k}}{8}\Lambda^3\psi_1\bar{\xi}^4) \tag{41}$$

Summarizing, Eq. (35) gives, for a certain value of the time at perturbation t_1, the real value of $\bar{\eta}$ as a function of the dimensionless wavenumber $\bar{\xi}$. The requisite for unstable growth of $\mathbb{S}_1$ is given by the condition $Re\,(\bar{\eta}) > 0$. Eq. (35) has three roots in $\bar{\eta}$, one real and two complex conjugates. Only the one having the greater positive real part has to be considered for the analysis of the dimensionless perturbation growth rate $\bar{\eta}^+$. Moreover, imposing the condition for maximum perturbation growth $\partial\bar{\eta}^+/\partial\bar{\xi} = 0$, the critical wavenumber $\bar{\xi}_c$ and the critical perturbation growth $\bar{\eta}_c^+$ are determined numerically.

It is important to note here that the stability analysis does not allow for calculation of the necking strain, but it allows identifying the dependence of necking strain with material behavior. Namely, the necking strain $\bar{\varepsilon}^p_{neck}$ correlates with the critical perturbation growth $\bar{\eta}_c^+$ as described by the authors (Vadillo et al., 2012; Rodríguez-Martínez et al., 2013b; Zaera et al., 2013b).

4. 3D Finite element modelling

The axisymmetric finite element model used to simulate the rapid stretching of a ductile cylindrical bar is based on that developed by Zaera et al. (2013b), but we present here its main features for completeness.

The numerical analyses are carried out using the finite element program ABAQUS/Explicit (Simulia, 2012). The dimensions of the cylindrical bar are $L_0 = 2 \cdot 10^{-2}\ m$ initial length, and $r_0 = 5 \cdot 10^{-4}\ m$ initial radius. Due to the symmetry of the model, only the $z \geq 0$ half of the specimen needs to be analyzed (see Fig.1). The bar was meshed using a total of 2000 four-node, thermally coupled, axisymmetric reduced integration elements (10 elements in the radial direction and 200 elements along the half-length), CAX4RT in ABAQUS notation, with an element aspect ratio equal to 1:1 (Fig.1). Neither geometrical nor material imperfections were introduced into the model, the numerical round-off being sufficient to perturb the stress and the strain fields (Rusinek and Zaera, 2007; Vadillo et al., 2012; Rodríguez-Martínez et al., 2013b).

The imposed loading conditions can be formulated as $V_z(r, L/2, t) = \dot{\varepsilon}_0 L_0/2$, $V_z(r, 0, t) = 0$. In order to avoid the spurious propagation of waves along the bar, caused by the application of these boundary conditions in a solid at rest showing elastic behavior, specific

initial conditions consistent with the boundary conditions are imposed, $V_r(r,z,0) = -\frac{\dot{\varepsilon}_0}{2}r$ and $V_z(r,z,0) = \dot{\varepsilon}_0 z$ (see Zaera et al. (2013b) for detailed explanation of these initial conditions).

Likewise, in order to avoid the abrupt jump in the stress field caused by application of the boundary conditions, the material flow has been initialized in the whole domain with a value of σ_z equal to the initial yield stress of the material (see Eqs. (21)). If neither the velocity nor the stress fields were initialized, for sufficiently high velocities the generated wave could induce by itself a neck (Needleman, 1991; Xue et al., 2008). Regarding initial thermal conditions, the initial temperature was set to 293 K in all cases.

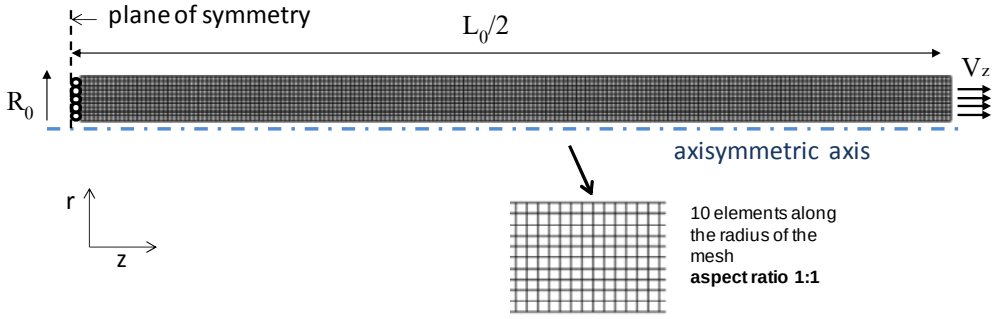

Figure 1: Finite element mesh and mechanical boundary conditions of the cylindrical bar, modeled as an axially symmetric specimen (Zaera et al., 2013b).

The set of equations describing the constitutive behavior of the material are implemented -using a fully coupled thermomechanical scheme- in the finite element code through a user subroutine following the integration scheme reported in Zaera et al. (2013b).

5. Results and discussion

Results of stability analysis and finite element simulations are presented, the goal being to asses the respective influence of microstructural and thermal softening effects on dynamic necking inception. The analysis is divided into two parts: (1) influence of microstructural softening effects on flow localization, (2) influence of thermal softening effects on flow localization.

U_{DRX} (MPa/m^3)			
$0.125U^*$	$0.25U^*$	$0.5U^*$	U^*

Table 2: Values of U_{DRX} used to analyse the influence of microstructural softening on dynamic necking. The range of values is taken following Osovski et al. (2013).

5.1. Influence of microstructural softening effects on dynamic necking inception

Following the procedure reported by Osovski et al. (2013), the material parameter controlling thermal softening is set to be constant $\alpha = \alpha^*$ (see Table 1) and the DRX threshold energy U_{DRX} is varied as illustrated in Table 2.

According to the material parameters listed in Table 1, Fig. 2 shows the dimensionless flow stress upon plastic strain for the values of U_{DRX} reported in Table 2. Below, some observations are reported:

- $U_{DRX} = 0.125U^*$: For plastic strains $\bar{\varepsilon}^p \lesssim 0.1$ slip is the main mechanism responsible for the plastic flow leading to visible strain hardening effects. Within the range $\bar{\varepsilon}^p \gtrsim 0.1$ the material develops DRX and strain hardening effects are cancelled. It has to be noted that strain softening effects are almost negligible.

- $U_{DRX} = 0.25U^*$: The stress-strain curve is largely similar to that shown for $U_{DRX} = 0.125U^*$. The difference resides in the plastic strain corresponding to the onset of DRX, which is slightly delayed in the present case. Thus, at large strains the yield stress corresponding to $U_{DRX} = 0.25U^*$ is a little larger than that corresponding to $U_{DRX} = 0.125U^*$. Strain softening effects are almost negligible.

- $U_{DRX} = 0.5U^*$: The material characteristic coincides with those reported for previous cases up to $\bar{\varepsilon}^p \approx 0.1$. Subsequently the material shows a dramatic increase in strain hardening and yield stress caused by the formation of twins. The maximum strain hardening is recorded for $\bar{\varepsilon}^p \approx 0.2$ (corresponding to the maximum rate of twinning formation). Twinning development stops for $\bar{\varepsilon}^p \approx 0.3$, this value of plastic strain

defines the onset of dynamic recrystallization which leads to strain softening and yield stress decrease.

- $U_{DRX} = U^*$: The stress-strain curve coincides with that reported for $U_{DRX} = 0.5U^*$ up to $\bar{\varepsilon}^p \approx 0.3$. Unlike in the case of $U_{DRX} = 0.5U^*$, now the onset of DRX is delayed until $\bar{\varepsilon}^p \approx 0.75$. This value of plastic deformation determines the onset of slight strain softening effects.

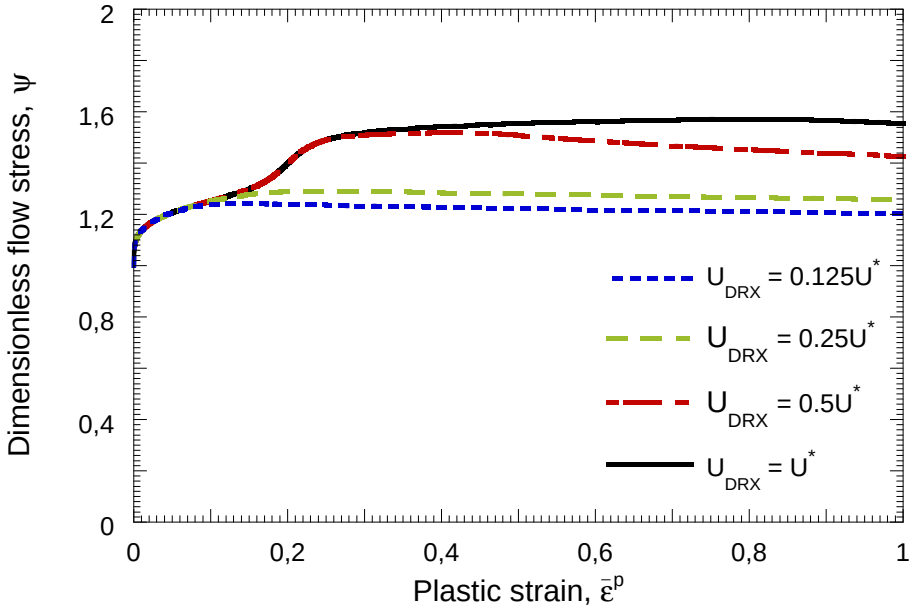

Figure 2: Dimensionless flow stress ψ versus equivalent plastic strain $\bar{\varepsilon}^p$ for different values of the DRX threshold energy: $U_{DRX} = 0.125U^*$, $U_{DRX} = 0.25U^*$, $U_{DRX} = 0.5U^*$ and $U_{DRX} = U^*$. To be noted that $\alpha = \alpha^*$ (see Table 1).

5.1.1. Stability analysis results

Next, the results obtained from the stability analysis are discussed. Here it is important to emphasize the relation between critical perturbation growth and necking strain. The stability analysis provides $\bar{\eta}_c^+$, whereas the necking strain will be obtained from finite element simulations.

Fig. 3 illustrates the dimensionless critical perturbation growth $\bar{\eta}_c^+$ versus plastic strain at perturbation ε_1 for the values of U_{DRX} listed in Table 2. Two different loading rates are analysed: $\dot{\varepsilon}_0 = 10^3\ s^{-1}$ in Fig. 3-a and $\dot{\varepsilon}_0 = 10^5\ s^{-1}$ in Fig. 3-b. It must be highlighted

that as the loading rate increases the critical perturbation growth decreases (to be noted from the different scale in the axis corresponding to $\bar{\eta}_c^+$ for Figs. 3-a and 3-b). The strain rate enhances the role played by inertia on the material response, stabilizing the plastic flow and delaying the onset of flow localization. Therefore, one should expect that as the loading rate increases, so does the necking strain (Zaera et al., 2013b).

Now we pay attention to the differences between the $\bar{\eta}_c^+ - \varepsilon_1$ curves corresponding to each value of U_{DRX} considered in this analysis. The observations reported below apply for any loading rate.

- $U_{DRX} = 0.125U^*$: For $\varepsilon_1 = 0$ the perturbation does not grow, strain hardening caused by deformation of the slip phase precludes strain localization. As plastic deformation proceeds, strain hardening effects are gradually reduced and the material yield stress increases. Both are destabilizing factors which promote flow localization and the perturbation starts to grow for $\varepsilon_1 \approx 0.05$. Any additional increase in plastic deformation causes a continuous rise of $\bar{\eta}_c^+$, i.e. material straining leads to a more unstable material favouring flow localization.

- $U_{DRX} = 0.25U^*$: The functional dependence of $\bar{\eta}_c^+$ upon ε_1 is almost identical to that reported for $U_{DRX} = 0.125U^*$ for the whole spectrum of ε_1 assessed since both cases show largely similar stress–strain characteristics, see Fig. 2.

- $U_{DRX} = 0.5U^*$: Identically to $U_{DRX} = 0.125U^*$ and $U_{DRX} = 0.25U^*$ the perturbation starts to grow for $\varepsilon_1 \approx 0.05$. Then, $\bar{\eta}_c^+$ increases until $\varepsilon_1 \approx 0.11$ when it reaches a relative maximum. From this point on, the critical perturbation growth decreases until $\bar{\eta}_c^+ = 0$ for $\varepsilon_1 \approx 0.16$ due to the drastic increase in strain hardening caused by twinning development (see Fig. 2). The material remains stable within the range $0.16 \lesssim \varepsilon_1 \lesssim 0.23$, which precludes flow localization. For $\varepsilon_1 \approx 0.23$ the material becomes again unstable and the perturbation grows. When $\varepsilon_1 \gtrsim 0.3$ the $\bar{\eta}_c^+ - \varepsilon_1$ relation obtained for $U_{DRX} = 0.5U^*$ does not differ significantly (neither qualitatively nor quantitatively) from those obtained for $U_{DRX} = 0.125U^*$ and $U_{DRX} = 0.25U^*$.

- $U_{DRX} = U^*$: The relation $\bar{\eta}_c^+ - \varepsilon_1$ looks very much like that reported for $U_{DRX} =$

$0.5U^*$ for the whole range of ε_1 examined since both cases show largely similar stress–strain characteristics, see Fig. 2.

Previous observations allow to draft two main conclusions:

1. If flow localization develops for values of strain $\varepsilon_1 < 0.3$, the necking strain will be presumably greater in the cases of $U_{DRX} = U^*$ and $U_{DRX} = 0.5U^*$ than in the cases of $U_{DRX} = 0.25U^*$ and $U_{DRX} = 0.125U^*$. At such low strains, twinning development stabilizes material behaviour (decreases $\bar{\eta}_c^+$) for $U_{DRX} = U^*$ and $U_{DRX} = 0.5U^*$ whereas DRX destabilizes material behaviour (increases $\bar{\eta}_c^+$) for $U_{DRX} = 0.25U^*$ and $U_{DRX} = 0.125U^*$.
2. If flow localization develops for values of strain $\varepsilon_1 \gtrsim 0.3$, the necking strain will be presumably similar for any value of U_{DRX} considered. At large strains the $\bar{\eta}_c^+$ – ε_1 relation shows little dependence on U_{DRX}. This suggests that, at sufficiently large strains, the values of U_{DRX} analysed are such that the resulting stress-strain characteristics show similar propensity to flow localization.

Next, the results of the finite element computations are presented and rationalized based on the linear stability analysis.

5.1.2. Finite element results

The localized necking strain $\bar{\varepsilon}^p_{neck}$ has been determined in the numerical computations following the procedure reported elsewhere (Triantafyllidis and Waldenmyer, 2004; Xue et al., 2008; Rodríguez-Martínez et al., 2013; Zaera et al., 2013b). The localized necking strain (from this point designated indistinctly as necking strain) is assumed as determined by the condition $d\bar{\varepsilon}^p/dt = 0$, where $\bar{\varepsilon}^p$ is measured within the unloading zone which surrounds the neck.

Fig. 4 shows the localized necking strain $\bar{\varepsilon}^p_{neck}$ measured for the values of U_{DRX} listed in Table 2 within a wide range of initial strain rates $10^2\ s^{-1} \leqslant \dot{\varepsilon}_0 \leqslant 10^5\ s^{-1}$. Consistent with the procedure followed in previous section, the results obtained for the values of U_{DRX} considered will be analysed separately:

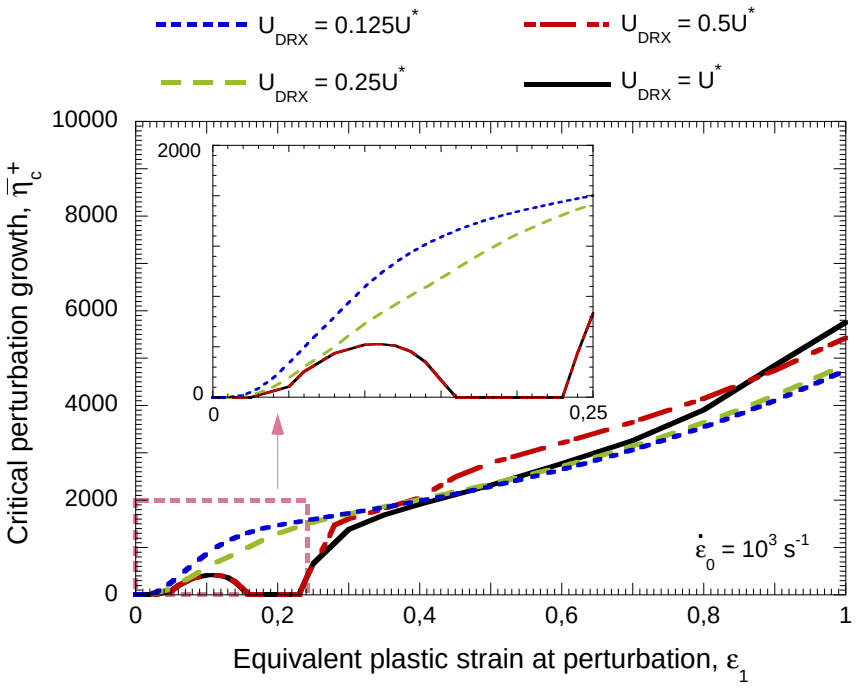

(a)

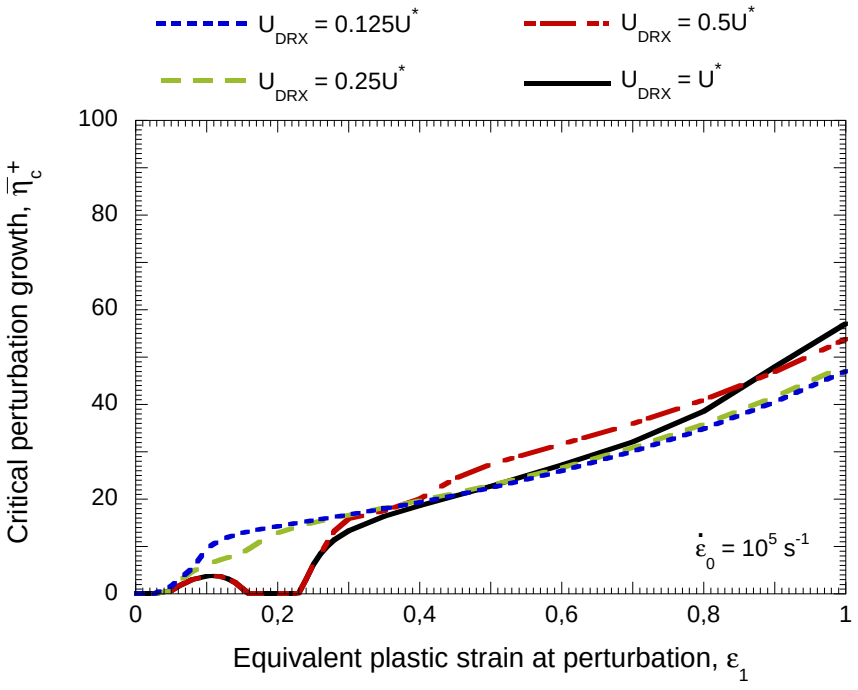

(b)

Figure 3: Critical perturbation growth $\bar{\eta}_c^+$ versus equivalent plastic strain at perturbation ε_1 for different values of the DRX threshold energy: $U_{DRX} = 0.125U^*$, $U_{DRX} = 0.25U^*$, $U_{DRX} = 0.5U^*$ and $U_{DRX} = U^*$. (a) $\dot{\varepsilon}_0 = 10^3\ s^{-1}$, (b) $\dot{\varepsilon}_0 = 10^5\ s^{-1}$. To be noted that $\alpha = \alpha^*$ (see Table 1).

- $U_{DRX} = 0.125U^*$: For $10^2\ s^{-1} \leqslant \dot{\varepsilon}_0 \lesssim 2 \cdot 10^3\ s^{-1}$ the necking strain shows very little increase with loading rate, being $\bar{\varepsilon}^p_{neck} \approx 0.05$. Note that this is the value of ε_1 reported in previous section for which the perturbation starts to grow. Consequently, flow localization is determined by strain hardening/softening effects. For $\dot{\varepsilon}_0 > 2 \cdot 10^3\ s^{-1}$ the necking strain experiences a continuous increase with loading rate. The necking strain does not correspond to the threshold strain required by the perturbation to grow, see Fig. 3, since the contribution of inertia is large enough to further delay strain localization. Therefore, flow localization becomes noticeably controlled by inertia.

- $U_{DRX} = 0.25U^*$: As expected from the stability analysis results, the functional dependence of $\bar{\varepsilon}^p_{neck}$ upon $\dot{\varepsilon}_0$ is largely similar to that reported for $U_{DRX} = 0.125U^*$ for the whole spectrum of loading rates assessed.

- $U_{DRX} = 0.5U^*$: For $10^2\ s^{-1} \leqslant \dot{\varepsilon}_0 \lesssim 2 \cdot 10^3\ s^{-1}$ the necking strain shows very little increase with loading rate, being $\bar{\varepsilon}^p_{neck} \approx 0.23$. This value was identified in the stability analysis as the threshold strain required by the perturbation to develop the second branch of growth, see Fig. 3. Interestingly, flow localization does not occur within the range of plastic strains corresponding to the first branch of perturbation growth. In fact, in the simulations, one can observe the onset of necking for $\bar{\varepsilon}^p_{neck} \approx 0.05$ (the beginning of the first branch of perturbation growth) but necking development is arrested as soon as the plastic strain reaches $\bar{\varepsilon}^p_{neck} \approx 0.16$ (the end of the first branch of perturbation growth). Necking preclusion homogenizes the plastic strains along the bar and flow localization becomes postponed until $\bar{\varepsilon}^p_{neck} \approx 0.23$ (the onset of the second branch of perturbation growth) when necking can develop since any further increase in plastic strain leads to material destabilization. Therefore, flow localization is mainly dictated by the strain hardening/softening effects. For $\dot{\varepsilon}_0 > 2 \cdot 10^3\ s^{-1}$ the necking strain shows a marked increase with loading rate. The necking strain does not correspond to the threshold strain required by the perturbation to develop the second branch of growth illustrated in Fig. 3, since the contribution of inertia is large enough to further delay strain localization. Therefore, flow localization

becomes again controlled by inertia. It has to be highlighted that, as predicted by the stability analysis, the results obtained for $U_{DRX} = 0.5U^*$ become very similar to those obtained for $U_{DRX} = 0.25U^*$ and $U_{DRX} = 0.125U^*$ for the largest loading rates considered (specifically when the loading rate is such that the necking strain exceeds 0.3).

- $U_{DRX} = U^*$: As expected from the stability analysis results, the relation $\bar{\varepsilon}^p_{neck} - \dot{\varepsilon}_0$ is very similar to that reported for $U_{DRX} = 0.5U^*$ for the whole spectrum of loading rates assessed.

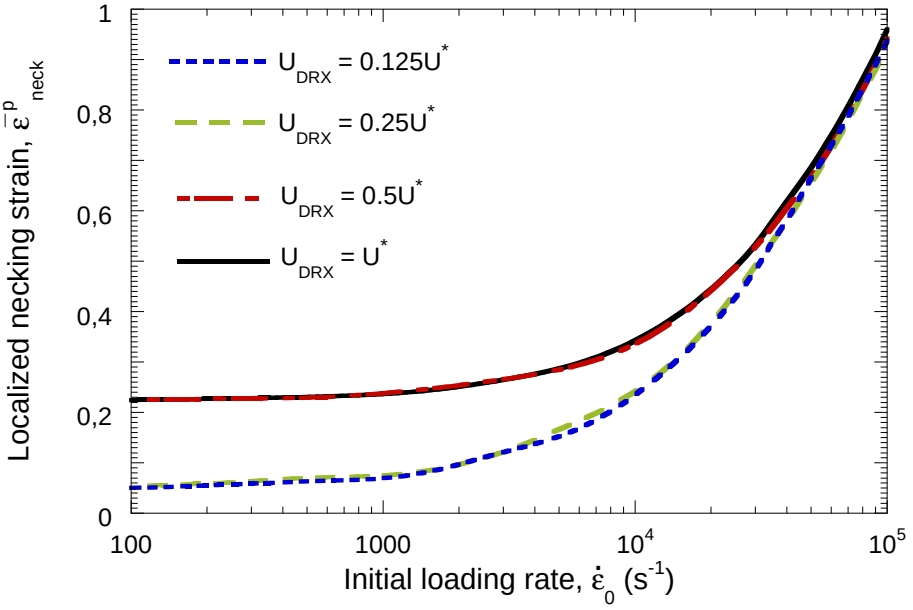

Figure 4: Localized necking strain $\bar{\varepsilon}^p_{neck}$ versus initial loading rate $\dot{\varepsilon}_0$ for different values of the DRX threshold energy: $U_{DRX} = 0.125U^*$, $U_{DRX} = 0.25U^*$, $U_{DRX} = 0.5U^*$ and $U_{DRX} = U^*$. To be noted that $\alpha = \alpha^*$ (see Table 1).

Two main conclusions are derived from previous observations:

1. At sufficiently low loading rates the necking strain is dictated by strain hardening/softening effects whereas inertia shows negligible influence on flow localization. This results in necking strains which are directly tied to the microstructural transformations experienced by the material.
2. At sufficiently high loading rates the material ductility to necking is essentially dictated by inertia whereas strain hardening/softening effects play a secondary role on

α (K^{-1})			
0	α^*	$4\alpha^*$	$8\alpha^*$

Table 3: Values of α used to analyse the influence of thermal softening on dynamic necking. The range of values is taken following Osovski et al. (2013).

flow localization. This results in necking strains which show negligible influence of the microstructural transformations experienced by the material.

5.2. Influence of temperature softening effects on dynamic necking inception

Following the procedure reported by Osovski et al. (2013), the DRX threshold energy is set to be constant $U_{DRX} = U^*$ (see Table 1) and the material parameter controlling thermal softening α is varied as illustrated in Table 3.

According to the material parameters listed in Table 1, Fig. 5 illustrates the dimensionless flow stress upon plastic strain for the values of α reported in Table 3. Below, some observations are reported:

- $\alpha = 0$: The material yield stress is assumed as temperature independent. Slip controls plastic flow within the range of plastic strains $\bar{\varepsilon}^p \lesssim 0.1$. Then, there is a rapid development of twinning which leads to a drastic increase of material strain hardening. $\bar{\varepsilon}^p \approx 0.2$ determines the point of maximum rate of twinning formation, further material straining leads to gradual reduction of strain hardening effects. Saturation of the stress-strain characteristic occurs for $\bar{\varepsilon}^p \approx 0.8$. This value marks the onset of DRX formation which in turn triggers slight material strain softening.

- $\alpha = \alpha^*$: The stress-strain curve is largely similar to that shown for $\alpha = 0$. The difference resides in the plastic strain value for which saturation of the stress-strain characteristic occurs. In the present case this occurs at $\bar{\varepsilon}^p \approx 0.75$ due to thermal effects. From this point on, material strain softening is clearly visible.

- $\alpha = 4\alpha^*$: Qualitatively the stress-strain curve looks like those described for $\alpha = 0$ and $\alpha = \alpha^*$. However, in the present case stress saturation occurs at $\bar{\varepsilon}^p \approx 0.55$ due

to the larger temperature sensitivity of the material. Further material straining leads to strain softening effects larger than those reported for $\alpha = 0$ and $\alpha = \alpha^*$.

- $\alpha = 8\alpha^*$: The stress-strain curve is very similar to those corresponding to $\alpha = 0$, $\alpha = \alpha^*$ and $\alpha = 4\alpha^*$. The larger temperature sensitivity brings the stress saturation to $\bar{\varepsilon}^p \approx 0.3$ and leads to material strain softening effects higher than those reported for $\alpha = 0$, $\alpha = \alpha^*$ and $\alpha = 4\alpha^*$.

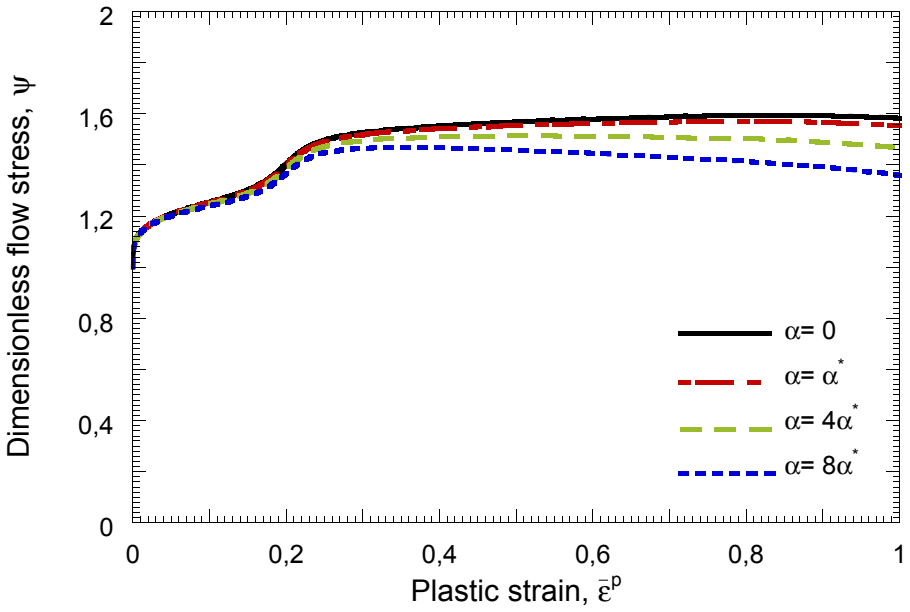

Figure 5: Dimensionless flow stress ψ versus equivalent plastic strain $\bar{\varepsilon}^p$ for different values of the temperature sensitivity parameter: $\alpha = 0$, $\alpha = \alpha^*$, $\alpha = 4\alpha^*$ and $\alpha = 8\alpha^*$. To be noted that $U_{DRX} = U^*$ (see Table 1).

5.2.1. Stability analysis results

Next, the results obtained from the stability analysis are discussed. Fig. 6 illustrates the dimensionless critical perturbation growth $\bar{\eta}_c^+$ versus plastic strain at perturbation ε_1 for the values of α listed in Table 3. Two different loading rates are analyzed: $\dot{\varepsilon}_0 = 10^3\ s^{-1}$ in Fig. 6-a and $\dot{\varepsilon}_0 = 10^5\ s^{-1}$ in Fig. 6-b.

It is important to remember here that the loading rate decreases the critical perturbation growth, thus stabilizing the plastic flow. We pay attention now to the differences between the $\bar{\eta}_c^+ - \varepsilon_1$ curves corresponding to each value of α considered in this analysis. The discussion conducted below applies for any loading rate.

- $\alpha = 0$: The material becomes unstable for $\varepsilon_1 \approx 0.05$. Then, $\bar{\eta}_c^+$ increases until reaching a relative maximum for $\varepsilon_1 \approx 0.11$. Subsequently, the material becomes gradually stabilized by the drastic increase in strain hardening caused by twinning development (see Fig. 5) until $\varepsilon_1 \approx 0.16$ when the condition $\bar{\eta}_c^+ = 0$ is reached. The perturbation does not grow within the range $0.16 \lesssim \varepsilon_1 \lesssim 0.23$, which precludes flow localization. For $\varepsilon_1 \approx 0.23$ the material becomes unstable again, further material straining causes continuous rise in $\bar{\eta}_c^+$.

- $\alpha = \alpha^*$: The relation $\bar{\eta}_c^+ - \varepsilon_1$ is qualitative very similar to that reported for $\alpha = 0$. The strain values for which the condition $\bar{\eta}_c^+ = 0$ is fulfilled remain practically the same. However, within the range of ε_1 for which the perturbation grows, the values of $\bar{\eta}_c^+$ registered in the present case are slightly higher than those obtained for $\alpha = 0$.

- $\alpha = 4\alpha^*$: The relation $\bar{\eta}_c^+ - \varepsilon_1$ is qualitative very similar to those reported for $\alpha = 0$ and $\alpha = \alpha^*$. The only difference resides in the values of $\bar{\eta}_c^+$ –within the ranges of ε_1 for which the perturbation grows– which are slightly larger in the present case.

- $\alpha = 8\alpha^*$: The relation $\bar{\eta}_c^+ - \varepsilon_1$ is almost identical to those described for previous cases. Again, the only difference resides in the values of $\bar{\eta}_c^+$ which are slightly larger in the present case.

Previous observations allow to derive two main conclusion:

1. Qualitatively, thermal effects play a negligible role on the $\bar{\eta}_c^+ - \varepsilon_1$ curves. For the material cases analyzed here, the range of plastic strains for which the perturbation growth is not affected by thermal softening. The condition of stability or instability of the material is dictated by the microstructural transformations which show great influence on the yield stress level and strain hardening of the material.
2. Quantitatively, thermal effects act as a destabilizing factor. Increasing temperature sensitivity triggers greater strain softening effects which in turn lead to larger values of $\bar{\eta}_c^+$ within the range of plastic strains for which the perturbation grows. However such increase of $\bar{\eta}_c^+$ is shown to be very limited for the material cases analyzed here.

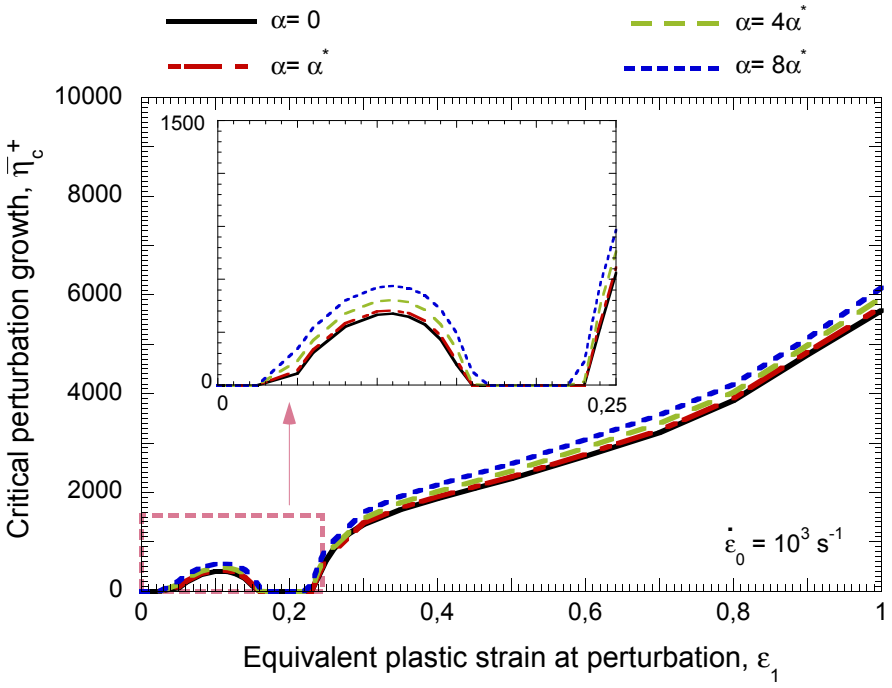

(a)

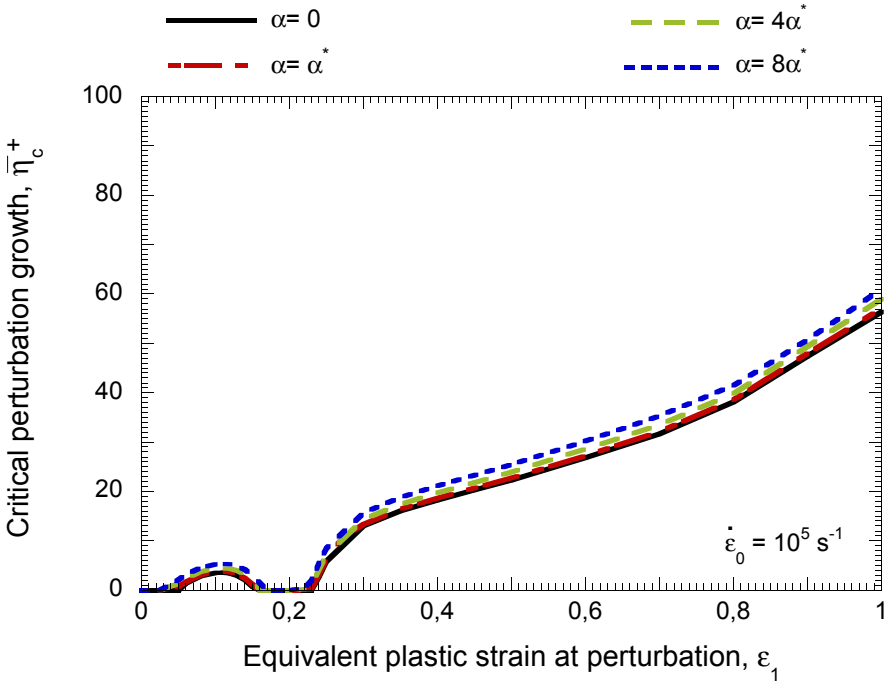

(b)

Figure 6: Critical perturbation growth $\bar{\eta}_c^+$ versus equivalent plastic strain at perturbation ε_1 for different values of the temperature sensitivity parameter: $\alpha = 0$, $\alpha = \alpha^*$, $\alpha = 4\alpha^*$ and $\alpha = 8\alpha^*$. (a) $\dot{\varepsilon}_0 = 10^3\ s^{-1}$, (b) $\dot{\varepsilon}_0 = 10^5\ s^{-1}$. To be noted that $U_{DRX} = U^*$ (see Table 1).

The value of $\bar{\eta}_c^+$ is mainly controlled by the microstructural transformations which show great influence on the yield stress level and strain hardening of the material.

This analysis suggests that the necking strain is largely independent of the thermal softening parameter, irrespective of the loading rate considered.

5.2.2. Finite element results

Next, the results obtained from the finite element computations are discussed. Fig. 7 shows the localized necking strain $\bar{\varepsilon}^p_{neck}$ measured for the values of α listed in Table 3 within a wide range of initial strain rates $10^2\ s^{-1} \leqslant \dot{\varepsilon}_0 \leqslant 10^5\ s^{-1}$. Consistent with the procedure followed in previous section, the results obtained for the values of α considered will be analysed separately:

- $\alpha = 0$: Within the range of loading rates $10^2\ s^{-1} \leqslant \dot{\varepsilon}_0 \lesssim 2 \cdot 10^3\ s^{-1}$ the necking strain shows very little increase with loading rate, being $\bar{\varepsilon}^p_{neck} \approx 0.23$. This value was identified in the stability analysis as the threshold strain required by the perturbation to develop the second branch of growth illustrated in Fig. 6. As reported in previous section, at low strain rates the necking strain is dictated by the strong influence that microstructural transformations have on yield stress and strain hardening of the material. For $\dot{\varepsilon}_0 > 2 \cdot 10^3\ s^{-1}$ the necking strain shows continuous increase with loading rate. The necking strain does not correspond to the threshold strain required by the perturbation to develop the second branch of growth illustrated in Fig. 7, since the contribution of inertia is large enough to further delay strain localization.

- $\alpha = \alpha^*$: The necking strain is largely similar to that obtained for $\alpha = 0$ within the whole range of loading rates considered.

- $\alpha = 4\alpha^*$: Identical comments to the previous case.

- $\alpha = 8\alpha^*$: Identical comments to the previous two cases.

Two main conclusions are derived from previous observations:

1. At low strain rates the necking strain is controlled by the strong influence of twinning and DRX on material yield stress level and strain hardening, playing thermal effects a negligible role.

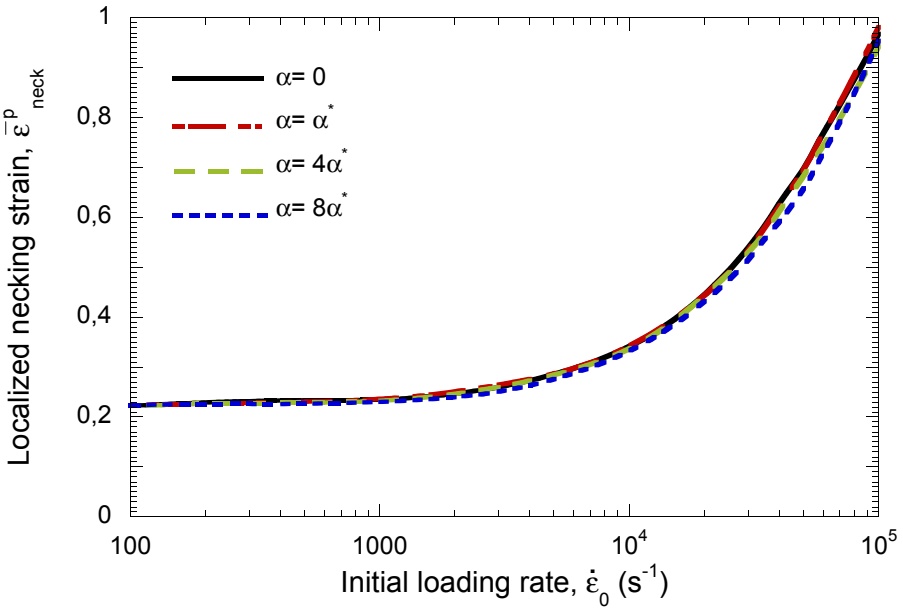

Figure 7: Localized necking strain $\bar{\varepsilon}^p_{neck}$ versus initial loading rate $\dot{\varepsilon}_0$ for different values of the temperature sensitivity parameter: $\alpha = 0$, $\alpha = \alpha^*$, $\alpha = 4\alpha^*$ and $\alpha = 8\alpha^*$. To be noted that $U_{DRX} = U^*$ (see Table 1).

2. At high strain rates the necking strain is mainly controlled by inertia irrespective of thermal effects.

This analysis suggests that in presence of microstructural transformations with strong influence on the stress-strain characteristics of the material like those considered in this analysis – i.e. twinning and DRX – thermal softening effects may play a minor role on material flow localization for any loading rate considered.

6. Discussion

The present paper provides an analytical investigation of the respective role of microstructural (phase transformation) and thermal softening mechanisms to the generation of dynamic instabilities. As such, it is a direct extension of the recent previous numerical study of Osovski et al. (2013), with the following major differences: The paper studies another type of instability, namely tensile (necking), as opposed to the previous study of shear localization. The approach adopted here is completely different: A one-dimensional stability analysis is performed analytically, albeit based on the same constitutive parameters used by Osovski et al. (2013). This analysis provides a new type of information, namely

the rate of perturbation growth and its modes, which is to be contrasted with the previous emphasis on the onset of shear localization. The one-dimensional analysis is then confronted to a fully coupled three dimensional numerical analysis of the necking phenomenon for one basic material (titanium alloy) whose physical properties are systematically varied. This study shows the various evolutions of the necking strain, when necking has been identified in the first stage as the perturbation itself, as a function of the strain rate. In that respect, the numerical part of this work bears some resemblance to the previous work of Osovski et al. (2013), with the following major differences: The first point that is emphasized is that of the dependence of the necking strain on the applied strain-rate. Our study shows that, whereas for the lower strain-rates, the necking strain is indeed the perturbation strain at which the perturbation exhibits a maximal growth rate (analytical result), the two strains differ significantly as soon as the strain rate grows beyond 10^3 s^{-1}. This point, which was not noted previously, is in perfect agreement with the previous results of Rodríguez-Martínez et al. (2013a) who showed that inertia has a dominant stabilizing role on the onset of the tensile instability. As such, while the previous study of Osovski et al. (2013) outlined two dominant regimes, one being the microstructural dominance, the second involving thermal softening, one sees here that a third regime overrules the previous two when the strain rate increases significantly, to a point where neither microstructural nor thermal softening effects are relevant any longer. In this regime, all the investigated nuances of material are no longer distinguishable. One main outcome of this study is the minor role played by thermal softening on the onset of the tensile instability, with respect to the dominant microstructural influence.

While one must be careful in generalizing this observation, the point remains definitely new and of interest. While dynamic shear instabilities, investigated e.g. by Osovski et al. (2013) were long primarily attributed to thermal softening, a point which prompted the study in question, the same cannot be claimed for the onset of tensile instability. One could argue here that provided necking occurs at relatively small tensile strains, the probability for material self-heating, assuming that the Taylor-Quinney coefficient of the material is well known, still remains rather small. Hence, one has to look for other destabilizing mechanisms, one of which being the microstructural evolutions studied in this work. One

can therefore rationalize the observed lack of thermal softening influence based on those physical premises. However, should there be no such phase transformations, such as DRX, and given the delaying influence of inertia at very high strain rates, one could expect that thermal softening plays some role on the onset of necking. The present results do not absolutely contradict this point, but as noted in Figs. 6-7, thermal softening is definitely not the dominant parameter here.

From a broader perspective, the following points should be mentioned. First, this analysis presents a framework to investigate the onset of dynamic instabilities, at this stage tensile necking. One can expect the similar framework to apply to other instabilities, such as (adiabatic) shear bands for example. The present analysis, comprises one important simplifying assumption, namely that the material is not strain rate sensitive. For the titanium alloy in question here, the experimental results show that this is not the case, however, this assumption must be made to facilitate the interpretation of the perturbation and numerical analyses results. Yet, when the current results are compared to the previous numerical work of Osovski et al. (2013) who considered a rate-sensitive material, one cannot really see a significant qualitative difference, a point that seems to indicate that the neglect of the rate sensitivity is not affecting the outcome of the analysis to a significant extent.

Finally, one should pay attention to the numerical approach employed in this work. Instead of solving the fully transient problem in which waves propagate throughout the specimen, the dynamic loading was applied by means of initialized velocity (and stress) fields. In this case, inertia (mass and velocity) is preserved, but waves do not propagate since there is no prescribed velocity jump. Consequently, this method allows for the separation of structural (inertia and wave related) and material (constitutive) effects in a simple and straightforward manner. Such a separation and its outcome is highly desirable for the kind of studies carried out here, as opposed to full transient analyses (Osovski et al., 2013) in which structural and material aspects were all analysed simultaneously. The current approach allows for a clear separation between material aspects of the problem in the lower strain-rate regime, which become structural in nature at the higher strain-rates where inertia prevails. To summarize the present study and its main results, a new stability analysis has been presented, based on previous physical observations and numerical

results, in which the emphasis is on the joint influence of the microstructural evolutions and thermal softening. The analytical study has defined the rate of growth of the critical mode as a function of those parameters, while the critical strain at which necking commences was calculated numerically. Although conducted from a radically different perspective, the present study supports and complements our previous work, showing the important role of microstructural softening at the expense of the thermal one, added to the dominant role of inertia as a stabilizing factor at very high strain rates, a point that was not previously considered in this specific case of dynamically necking phase transforming materials and their stability.

7. Conclusions

A stability analysis has been presented, that includes two competing deformation micromechanisms, twinning and dynamic recrystallization. The analysis is completed by a numerical simulation of dynamic necking in a tensile bar. The specific formulation of the initial and prescribed loading conditions of the fully coupled thermomechanical problem at hand, allow for a clear separation of the material and structural aspects of the problem.

In the lower range of strain rates (up to about 10^3 s^{-1}) the analysis shows a clear influence of the microstructural mechanisms on the perturbation growth (necking). As expected, twinning stabilizes the material whereas DRX promotes localization. On the other hand, thermal softening is shown to have a minor influence, if at all, on the onset of the tensile localization. Those results are in full agreement with the previous work of Osovski et al. (2013) who studied a similar related problem (shear) using a purely numerical approach in which wave propagation was accounted for.

In the higher strain rate regime, the results show that inertia governs the onset of the localization, by postponing neck formation. In this case, which was not addressed previously, one can notice that the thermomechanical characteristics of the bar play a very minor role to a point where all materials and thermal couplings combinations collapse into a single curve. This result is consistent with previous work about multiple necking in metallic rings subjected to very high strain rates (Rodríguez-Martínez et al., 2013a).

It is expected that the approach proposed here can be applied in the future to the

analysis of the dynamic shear localization case, as in Molinari (1997).

Acknowledgements

This paper is dedicated to Professor Alain Molinari for his outstanding contributions in the field of Solids Mechanics.

The authors are indebted to the *Ministerio de Ciencia e Innovación de España* (Projects DPI/2011-24068 and DPI/2011-23191) for the financial support.

D. Rittel acknowledges the support of University Carlos III of Madrid with a Cátedra de Excelencia funded by Banco Santander during academic year 2011-2012.

Bailey, J., Hirsch, P., 1962. The recrystallization process in some polycrystalline metals. Proc Roy Soc A 267.

Bridgman, P. W., 1952. Studies in large plastic flow and fracture, with special emphasis on the effects of hydrostatic pressure. Scientific papers, vol. 1 mechanics of solids; p:9-37. New York:McGraw-Hill Book Company, Inc.

Brown, A., Bammann, D., 2012. Validation of a model for static and dynamic recrystallization in metals. International Journal of Plasticity 32-33, 17–35.

Ding, R., Guo, Z., 2001. Coupled quantitative simulation of microstructural evolution and plastic flow during dynamic recrystallization. Acta Mater 49, 3163–3175.

Fan, X., Yang, H., 2011. Internal-state-variable based self-consistent constitutive modeling for hot working of two-phase titanium alloys coupling microstructure evolution. International Journal of Plasticity 27, 1833–1852.

Fressengeas, C., Molinari, A., 1985. Inertia and thermal effects on the localization of plastic flow. Acta Metallurgica 33, 387–396.

Ganapathysubramanian, S., Zabaras, N., 2004. Deformation process design for control of microstructure in the presence of dynamic recrystallization and grain growth mechanisms. International Journal of Solids and Structures 41, 2011–2037.

Klepaczko, J. R., 1968. Generalized conditions for stability in tension test. International Journal of Mechanical Sciences 10, 297–313.

Li, H., Wu, C., Yang, H., 2013. Crystal plasticity modeling of the dynamic recrystallization of two-phase titanium alloys during isothermal processing. International Journal of Plasticity DOI: http://dx.doi.org/10.1016/j.ijplas.2013.05.001.

Medyanik, S., Liu, W., Li, S., 2007. On criteria for dynamic adiabatic shear band propagation. Journal of the Mechanics and Physics of Solids 55, 1439–1461.

Molinari, A., 1997. Collective behaviour and spacing of adiabatic shear bands. Journal of the Mechanics and Physics of Solids 45, 1551–1575.

Needleman, A., 1991. The effect of material inertia on neck development. In: Yang, W.H. (Ed.), Topics in Plasticity. AM Press, Ann Arbor, MI, 151–160.

Osovski, S., Nahmany, Y., Rittel, D., Landaub, P., Venkert, A., 2012a. On the dynamic character of localized failure. Scripta materialia 67, 693–695.

Osovski, S., Rittel, D., 2012. Microstructural heterogeneity and dynamic shear localization. Applied Physics Letters 101, 211901.

Osovski, S., Rittel, D., Landau, P., Venkert, A., 2012b. Microstructural effects on adiabatic shear band formation. Scripta Materialia 66, 9–12.

Osovski, S., Rittel, D., Venkert, A., 2013. The respective influence of microstructural and thermal softening on adiabatic shear localization. Mechanics of Materials 56, 11–22.

Qu, J., Jin, Q., Xu, B., 2005. Parameter identification for improved viscoplastic model considering dynamic recrystallization. International Journal of Plasticity 21, 1267–1302.

Rittel, D., Landau, P., Venkert, A., 2008. Dynamic recrystallization as a potential cause for adiabatic shear failure. Physical Review Letters 101, 165501.

Rittel, D., Ravichandran, G., Venkert, A., 2006. The mechanical response of pure iron at high strain rates under dominant shear. Materials Science and Engineering A 432, 191.

Rittel, D., Wang, Z., 2008. Thermo-mechanical aspects of adiabatic shear failure of AM50 and Ti6Al4V alloys. Mechanics of Materials 40, 629–635.

Rodríguez-Martínez, J. A., Rittel, D., Zaera, R., Osovski, S., 2013. Finite element analysis of AISI 304 steel sheets subjected to dynamic tension: the effects of martensitic transformation and plastic strain development on flow localization. International Journal of Impact Engineering 54, 206–216.

Rodríguez-Martínez, J. A., Vadillo, G., Fernández-Sáez, J., Molinari, A., 2013a. Identification of the critical wavelength responsible for the fragmentation of ductile rings expanding at very high strain rates. Journal of the Mechanics and Physics of Solids 61, 1357–1376.

Rodríguez-Martínez, J. A., Vadillo, G., Zaera, R., Fernández-Sáez, J., 2013b. On the complete extinction of selected imperfection wavelengths in dynamically expanded ductile rings. Mechanics of Materials 60, 107–120.

Rusinek, A., Zaera, R., 2007. Finite element simulation of steel ring fragmentation under radial expansion. International Journal of Impact Engineering 34, 799–822.

Simulia, 2012. ABAQUS/Explicit User's Manual, version 6.12 Edition. Dassault Systèmes, Providence, USA.

Tanner, A., McDowell, D., 1999. Deformation, temperature and strain rate sequence experiments on OFHC Cu. International Journal of Plasticity 15, 375–399.

Triantafyllidis, N., Waldenmyer, J. R., 2004. Onset of necking in electro-magnetically formed rings. J Mech Phys Solids 52, 2127–2148.

Vadillo, G., Rodríguez-Martínez, J. A., Fernández-Sáez, J., 2012. On the interplay between strain rate and strain rate sensitivity on flow localization in the dynamic expansion of ductile rings. International Journal of Solids and Structures 49, 481–491.

Walsh, J. M., 1984. Plastic instability and particulation in stretching metals jets. Journal of Applied Physics 56, 1997–2006.

Xue, Z., Vaziri, A., Hutchinson, J. W., 2008. Material aspects of dynamic neck retardation. Journal of the Mechanics and Physics of Solids 56, 93–113.

Zaera, R., Rodríguez-Martínez, J. A., Rittel, D., 2013a. On the Taylor-Quinney coefficient in dynamically phase transforming materials. Application to 304 stainless steel. International Journal of Plasticity 40, 185–201.

Zaera, R., Rodríguez-Martínez, J. A., Vadillo, G., Fernández-Sáez, J., 2013b. Dynamic necking in materials with strain induced martensitic transformation. Journal of the Mechanics and Physics of Solids, Submitted for Publication.

Zhou, F., Molinari, J. F., Ramesh, K. T., 2006. An elasto-visco-plastic analysis of ductile expanding ring. Int J Impact Eng 33, 880–891.